FACTA UNIVERSITATIS
Series: **Electronics and Energetics** Vol. 36, N° 2, June 2023, pp. 159-170
https://doi.org/10.2298/FUEE2302159S

Original scientific paper

INVESTIGATION OF DYE-SENSITIZED SOLAR CELL PERFORMANCE BASED ON VERTICALLY ALIGNED TiO_2 NANOWIRE PHOTOANODE *

Biraj Shougaijam, Salam Surjit Singh

Department of Electronics and Communication Engineering,
Manipur Technical University, Takyelpat-795004, Manipur, India

Abstract. *In this work, we present our results related to the development of Dye-Sensitized Solar Cells (DSSCs) based on vertically aligned TiO_2-nanowire (NW) and Ag nanoparticle (NP) assisted vertically aligned TiO_2-NW (TAT) photoanode fabricated by the glancing angle deposition (GLAD) technique on fluorine doped thin oxide (FTO) substrates. The scanning electron microscopy (SEM) analysis reveals that the Ag-NP assisted vertically aligned TiO_2-NW photoanode was successfully deposited on FTO substrates. The average length and diameter of the NW have been measured to be ~ 350 nm and ~ 90 - 100 nm, respectively. Moreover, transmission electron microscopy (TEM) and X-ray diffraction (XRD) manifest the presence of small crystals of TiO_2 and Ag. Further, the absorption spectrum analysis reveals that the incorporation of Ag-NP in TiO_2-NW increases absorption in the visible region, but decreases the efficiency of the cell after the incorporation of the nanoparticle. The calculated bandgap of the annealed Ag-NP (30 nm) assisted TiO_2-NW (TAT@30nm) sample from the photoluminescence (PL) graph is ~ 3.12 eV. Finally, it is observed that the TiO_2-NW based DSSC device shows better performance in terms of photo conversion efficiency (PCE) compared to the TAT@30nm photoanode based device, with an efficiency of ~0.61 % from the former and ~ 0.24 % from the latter. This reduction in the efficiency of TAT@30nm based devices is due to the larger size of Ag-NP, in which the nanoaprticle acts as an electron sink and acts as a blocking layer.*

Key words: *DSSCs, e-beam, nanowire, nanoparticle, TiO_2*

Received July 09, 2022; revised August 13, 2022; accepted September 05, 2022
Corresponding author: Biraj Shougaijam
Department of Electronics and Communication Engineering, Manipur Technical University, Takyelpat-795004, Manipur, India
E-mail: biraj.sh89@gmail.com
* An earlier version of this paper was presented at the International Conference on Micro/Nanoelectronics Devices, Circuits and Systems (MNDCS 2022), January 29-31, 2022, National Institute of Technology Silchar, India [1]

1. INTRODUCTION

The number of natural disasters is rising daily due to the rapid climate change in the last few decades, directly or indirectly caused by carbon emissions from fossil fuels and the destruction of forest areas. Therefore, it is important to develop a sustainable energy conversion device to overcome the issue of increasing energy demand. Fossil fuels are one of the main sources of energy that will eventually run out, which will have an effect on the environment and the ecosystem in the area. As a result, scientists are always working to improve renewable energy sources like hydroelectricity, solar energy and wind energy. Since a significant amount of sunlight penetrates the earth's surface, solar cells, among other energy sources, play a significant part in the generation of electrical energy. Lots of design and development have been done on photovoltaic technology to maximize the conversion efficiency of sunlight. The most commonly used solar cell materials are silicon, perovskites, graphene, III-V nitrites and organic dyes [1-6]. Among these, Dye-Sensitized Solar Cells (DSSCs) became attractive after O'Regan and Gratzel's reported the outstanding properties of DSSCs like the multicolor option, easy integration into building architecture, ease of fabrication, low cost and affordability [7]. Similar to how plant chlorophyll performs photosynthesis, this solar cell's operation relies on the photo-electrochemical reaction, in which the dye molecule acts as a molecular electron pump by trapping the light. When light falls on the surface of the cell, the excited dye molecule is oxidized and transferring those excited electrons into the conduction band of a wide bandgap semiconductor, such as nanostructured TiO_2. The excited electron in the TiO_2 nanostructure is then transported to the counter electrode by the process of diffusion through the external circuit. Again, the oxidized dye molecule present inside the cell is regenerated from iodine present in the redox electrolyte medium and further regenerated from iodine by reduction of triiodide on the counter electrode [8]. The four different modules that make up DSSCs are photoanode, dye, electrolyte, and counter electrode. Among these, the photoanode is crucial to the process of photon conversion and the dye sensitizer influences how well the DSSCs work. The sensitizer/dye should possess broad and strong absorption from the visible to the near region. Ruthenium compound is the most commonly used efficient and stable dye. Even though these dyes have some disadvantage compared to Eosin-Y and porphyrin, they have excellent electron injection, higher absorption in the visible range, good stability and efficient charge transfer, thereby giving the highest efficiency [9, 10].

Moreover, TiO_2 has a high bandgap, resistance to photo corrosion, and nontoxicity compared to other metal oxides like ZnO_2, SnO_2, Cu_2O, WO_3 and In_2O_3 [11-12]. Naturally, TiO_2 crystal, which belongs to the transition metal oxides, can assume any of the three forms, i.e., anatase, rutile or brookite [13-14]. Anatase TiO_2 is mainly employed to create photoanodes for DSSCs because of its higher charge transport and stability. The power conversion efficiency (PCE) of the DSSCs is significantly impacted by the form and size of the TiO_2 nanoparticle. TiO_2 is a chemically inert substance because it has a bandgap of ~ 3.2 eV or less and does not induce chemical reactions in the absence of light. Due to scaling laws, the chemical and physical properties of nanomaterials change as their geometrical dimension decreases [15]. So, there has been recent progress in the synthesis of TiO_2 nanomaterial like nanorods (NRs), nanowires (NWs) and nanotubes (NTs), which possess different properties because of the different synthesis techniques, unique nanostructure, and high surface-to-volume ratio that enhance the delocalized carrier charge particle, thereby

increasing the charge transportation. This 1D nanostructure can be used in designing photoanodes for the DSSCs application, which can enhance the efficiency through rapid electron transport.

Nanomaterial synthesis can be done in different ways, like the sol-gel method, the hydrothermal method, chemical vapour deposition (CVD) and physical vapour deposition (PVD) techniques, etc. [16-17]. Furthermore, TiO_2-NW enhanced the performance of the energy-sensing because of more reaction sites due to the high surface area and larger extension of the depletion region. In addition to that, TiO_2-NW has confined conductive channels which can reduce charge recombination, hence enhancing charge transportation as compared to other bulk structures. Yang *et al.* reported that porous TiO_2 TF was deposited by glancing angle deposition (GLAD) using e-beam deposition. Also, it was reported that TiO_2 film has the largest internal surface area, which enhances the dye absorption of the DSSCs [18]. Wong *et al.* reported that TiO_2 photoanodes were prepared using the e-beam technology. It is also observed that the efficiency of 6.1% was achieved at an inclined GLAD angle of 73º which improves the light trapping nature of the TiO_2 photoanode as it is a columnar structure [19]. The highest reported PCE of DSSCs is ~ 14.2 %, which is fabricated using the chemical process on screen-printed TiO_2 film [20]. Even though the efficiency of the DSSCs is much lower than that of Si solar cells, they have remarkable performance under low light intensity, which can be used in indoor lighting. So, in this work, the GLAD method was used to grow vertically aligned TiO_2-NW as photoanodes on fluorine-doped thin oxide (FTO) for DSSC application without using any catalyst. Furthermore, it should be noted that the GLAD can be used to precisely control the shape, size, and thickness of the nanostructure [21]. The vertical TiO_2 nanostructure achieved from GALD deposition enhances the efficiency by shortening the electron pathway through the vertical TiO_2-NW. Further, an attempt has been made to put Ag metal nanoparticles in the middle of the TiO_2-NW to enhance the photon absorption through surface plasmon resonance (SPR). The SPR effect mainly depends on the type of metal used, its shape and the size of the metal nanoparticle. Both Ag and Au exhibit a strong SPR effect in the visible region. However, the cost of the Ag metal is comparatively lower as compared to Au. Again, Ag-NP is highly stable and can withstand corrosion and less oxidized [22]. It is noteworthy to mention that the Ag nanoparticle can be used in various applications like supercapacitors, biosensors and other optoelectronic applications, etc [23-25].

Therefore, an effort is made to develop DSSC based on TiO_2-NW and Ag-NP embedded vertical TiO_2-NW photoanodes deposited by the GLAD method on FTO substrates for the DSSC application. The samples were analyzed using scanning electron microscopy (SEM), Transmission Electron Microscopy (TEM) and X-ray diffraction (XRD) (RigaKu Ultima IV, CuKa radiation, k = 0.1540) analysis for morphology and structural analysis, respectively. Finally, the performance of two types of DSSCs, i.e., TiO_2-NW and Ag-NP assisted TiO_2-NW photoanode based devices, is analyzed.

2. Experimental Details

2.1. Materials

Both the TiO_2 and Ag (both 99.999% pure) were procured from Tecnisco Advanced Materials Pte Ltd, Singapore. N719 Ruthenium dye sensitizer (95% pure) was purchased from SRL Pvt. Ltd, FTO/glass (12-14 Ω/cm^2) from MTI Corporation, USA and Iodolyte

HI-30 electrolyte were purchased from Solaronix, Switzerland. For the deposition of the TiO_2 and Ag, the material is loaded into the crucible and put into the evaporation chamber. Before creating the vacuum, the chamber was cleaned properly by applying acetone. Further, the vacuum is created inside the chamber and the samples are inclined at 81° during the NW and NP deposition.

2.2. Photoanode preparation

FTO glass substrates having a resistivity of ~ 12-14 ohm/cm^2 were properly cleaned sequentially by rinsing them in deionized water (DI) (Oxford Lab Fine Chem LLP (CAS No. 7732-18-5)) for 1 minute each and drying them in the open air for 5 minutes before putting them inside the chamber. The vertically oriented TiO_2-NW and Ag-NP assisted vertically aligned TiO_2-NW (TAT) are deposited on FTO coated glass substrates by the GLAD using an e-beam evaporator (Model No. Smart Coat 3.0, HHV India). This GLAD mechanism, which is installed inside the chamber, allows the change of the angle by moving the axis of it. In our previous work, the details of the fabrication process of TiO_2-NW and TAT samples were discussed [21]. Here, the process is explained in brief. The samples are kept at an inclined angle of 81° and rotated at 30 rpm to form a vertically aligned TiO_2 nanostructure. In the first round of deposition, TiO_2-NW (350 nm) samples were deposited on an FTO-coated glass (1 cm x 1 cm) substrate by employing the GLAD method. For another group of samples, TiO_2-NW (175 nm) was initially deposited on glass (1 cm x 1 cm). Further, Ag-NP (30 nm) was deposited above the TiO_2-NW (175 nm). Again, TiO_2-NW (175 nm) was deposited above the Ag-NP (30 nm)/TiO_2-NW (175 nm). Finally, we achieved the staking of TiO_2-NW (175 nm)/Ag-NP (30 nm)/TiO_2-NW (175 nm) (TAT@30nm) samples by employing the GLAD method. For every TiO_2 (30 nm) deposition, deposition was done for 12 minutes at a rate of ~ 0.6 Å/sec and the Ag (30 nm) deposition rate was kept constant at 0.8 Å/sec for 7 minutes. The deposition rate and thickness of the deposited film were monitored through a digital thickness monitoring system in all the deposition process to control the film thickness precisely. Similarly, vertically aligned TiO_2-NW with Ag 60 nm (TAT@60nm) and Ag 90 nm (TAT@90nm) samples are prepared using the same process and parameters. All these processes are performed under high vacuum conditions of ~ 2 x 10^{-5} mbar. The pressure of the chamber was maintained at ~ 6 x 10^{-6} mbar before the start of deposition. However, during the deposition, the pressure drops to ~ 2 x 10^{-5} mbar. Further, the photoanode samples for DSSCs fabrication are annealed at 500 ℃ for 3 hours. The samples were cooled down slowly and processed for dye loading.

2.3. Dye Preparation and Counter Electrode Preparation

6mg of N719 (95%, SRL Pvt. Ltd.) dye salt powder is mixed with a 0.5 mM concentration of ethanol using a vortex (Ependorf MixMate) at 200 rpm for 20 minutes to make 10 ml of N719 dye solution. The resulting dye solution is kept for 1 day for stabilization, as shown in Fig. 1 (inset). Fig. 1 shows the absorption peak of the N719 sample being measured using a UV-Vis spectrophotometer (AN-UV-6500N ANTech), which reveals four bands at ~ 504 nm, ~ 376 nm and ~ 308 nm, with a shoulder peak at ~ 252 nm. The two peaks in the visible band are attributed to metal-to-ligand charge transfer (MLCT).

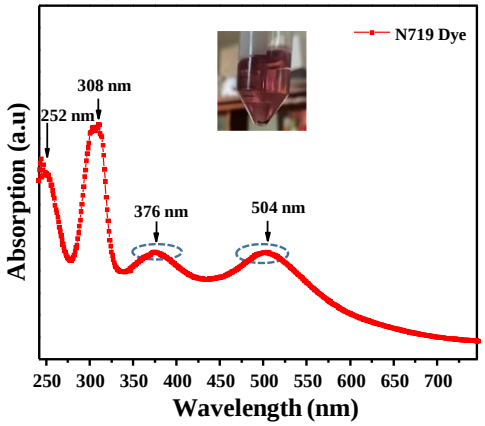

Fig. 1 Shows optical absorption spectrum of the N719 dye sample

The TiO_2-NW and TAT coated FTO glass samples are immersed in the N719 dye for 24 hours, which is kept at room temperature in a dark room. To remove the excess dye, the TiO_2 photoanode sample is washed gently with ethanol after taking it out of the dye solution and dried for 3 minutes in the open air. Again, Plastisol T/SP paste from the solaronix was coated on the FTO substrate using the doctor-blade technique for making the counter electrode (CE). Here, the 3M scotch tape covers all four edges of the sample by keeping a 2 x 2 cm^2 space at the centre of the FTO glass. This sample is placed in the furnace for annealing at 450ºC for 1 hour, which will activate the Pt particles.

2.4. Fabrication of DSSCs

The dye-sensitized TiO_2 photoanode and Pt-coated counter electrode were preheated at 100 °C before being sandwiched together. This pretreated process will remove the moisture present on the surface of the photoanode and counter electrode. Further, the Pt activated counter electrode is sandwiched and sealed with the TiO_2 photoanode by using a paper clip to complete the DSSCs module. Lastly, the electrolyte solution was introduced in between the electrodes by capillary action.

3. Results and Discussion

3.1. SEM Analysis

The morphology of the as-deposited TAT@30nm sample was analyzed using a SEM instrument, as shown in Fig. 2 which shows the successful deposition of TAT@30nm nanowires. The magnified SEM image of TAT@30nm sample is shown in Fig. 2(b). The larger diameter nanowires indicated by dotted circle, shown in Fig. 2(b), are built by cluster formation through shadowing effects during the deposition [26]. The average top diameter of the TAT@30nm was measured and calculated from the magnified SEM image and found to be ~ 72 nm, as shown in Fig. 2(c). Fig. 2(d) shows the cross-sectional image of TAT@30nm. This image proves that vertical TAT@30nm is successfully grown onto the FTO substrate by employing the GLAD technique. It also reveals the

presence of Ag-NPs, which are indicated by blue dotted circles in the middle of the NWs. The height of the TAT nanowire is ~337 nm.

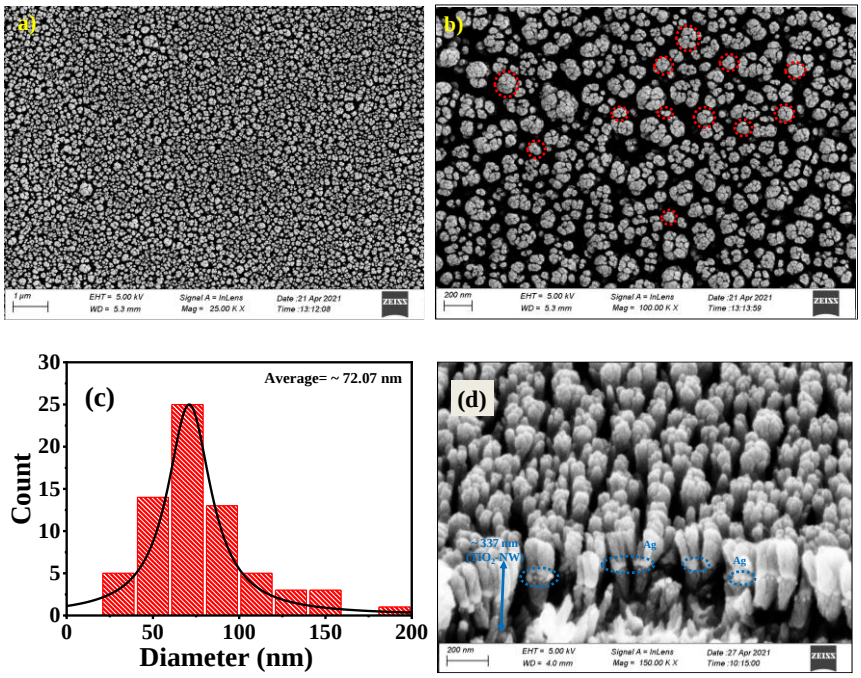

Fig. 2 (a) The SEM image of the as-deposited TAT@30nm, (b) Represent the magnified image showing the porous nature of the sample and (c) Showing the calculated average diameter, (d) a cross-sectional image of the TAT@30nm sample

These vertical nanostructures enhanced the efficiency of the DSSC solar cell by enhancing the surface area of the active layer as compared to thin-film [27]. Moreover, the vertical nanostructures have beneficial effects for DSSCs, since they have antireflection properties through the nanostructures that efficiently trap more light. Therefore, this method can be employed for developing high surface area photoanode nanostructures for DSSC applications and other optoelectronic applications.

3.2. TEM Analysis

For TEM analysis, the TiO_2 nanostructure layer deposited on the glass substrate was scrapped out using a doctor blade, which dispersed the scrapped-out powder into the acetone in a vial and ultrasonically sonicated the sample properly for a few minutes for good dispersion. Finally, place a drop of sonicated solution onto the TEM grid for TEM analysis. The TEM analysis of the TiO_2 and TAT samples is shown in Fig. 3 (a) and (b). The TiO_2-NWs are successfully grown using the GLAD technique, as shown in Fig. 3(a). The typical length measured from the nanowire image is ~ 259 nm and the arrow mark indicates the growth direction. Further, the TEM image of TAT sample manifests the presence of Ag-NP assisted at the mid of the TiO_2-NW. The HR-TEM images in inset (1) and (2) of Fig. 3(b) show the

presence of Ag crystal and TiO_2 crystal. The measured lattice constant from the inset (1) is found to be ~ 0.35 nm, which corresponds to (101) crystal plan of anatase TiO_2 (JCPDS No. 75-1753). From the inset (2), the measured lattice constant is found to be ~ 0.24 nm in the related crystal plane (111) of the Ag crystal (JCPDS No. 04-0783).

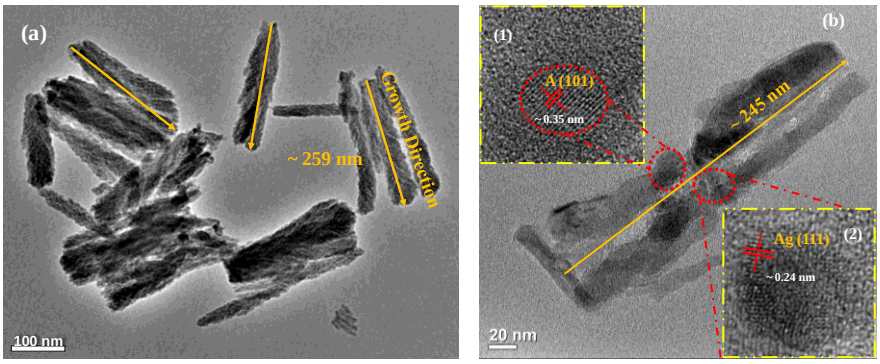

Fig. 3 (a) The TEM image of the as deposited TiO_2-NW, b) TEM image of annealed TAT@30nm and the inset represent the magnified HR-TEM image

3.2.1 XRD analysis

The as-deposited TiO_2-NW and Ag-NP (30 nm, 60 nm and 90 nm) assisted vertically aligned TiO_2-NW samples are analyzed by X-ray diffraction (XRD). Fig. 3(a) shows the XRD results of the as-deposited TiO_2-NW, TAT@30nm, TAT@60nm, and TAT@90nm samples. The weak peaks observed at 2θ = 25.76˚, 37.58˚, 48.4˚ and 63.4˚ are attributed to TiO_2 crystals with the corresponding orientation of (101), (103), (200) and (204), respectively (JCPDS No. 75-1753). The weak peaks may correspond to the small grain size of TiO_2 crystal grains. Again, the peaks at 38.27˚, 34.72˚ and 77.33˚ are related to the (111), (220) and (310) planes of Ag crystals (JCPDS No. 04-0783).

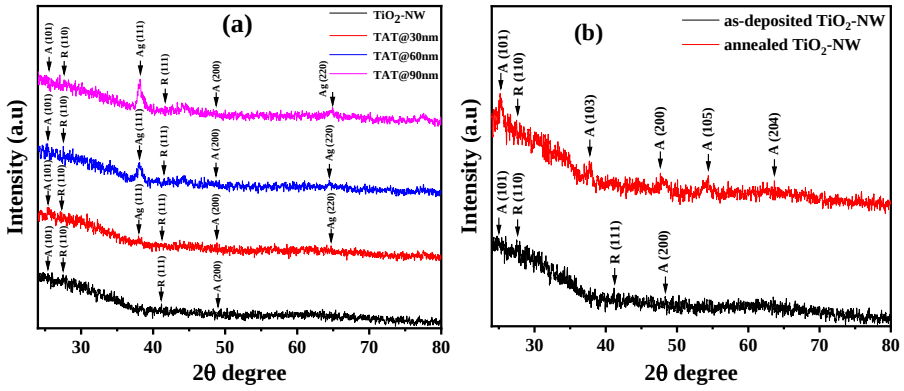

Fig. 4 (a) Shows the XRD results of TiO_2-NW, TAT@30nm, TAT@60nm, and TAT@90nm samples deposited at room temperature and (b) shows the XRD peak results for as-deposited TiO_2-NW and annealed TiO_2-NW

The annealing of TiO_2-NW improves the crystalline structure of TiO_2, as shown in Fig. 4(b). Oblique deposition of titanium oxide layers for DSSCs is done by using reactive e-beam deposition, which has the same weak peak. Further, as-deposited TiO_2 film was annealed for 3 h at 500 ˚C to produce crystalline TiO_2 [28].

3.3. UV-Vis Spectroscopy and Photoluminescence Spectroscopy

The optical properties of TiO_2-NW and TAT specimens fabricated on an FTO substrate were analyzed in the wavelength range of 340 nm to 800 nm using a UV-Vis spectrophotometer. The recorded absorption intensity of the sample is shown in Fig. 5 (a). The absorption spectrum of TiO_2-NW shows a higher absorption peak in the ultraviolet range. This peak may be attributed to electron excitation from the outermost valence band (VB) to the conduction band (CB) of the TiO_2 [29]. Moreover, the absorption spectrum of the TiO_2-NW is significantly enhanced in the visible region after the incorporation of different NP sizes, i.e., 30 nm, 60 nm and 90 nm. This significant improvement at around 400 to 600 nm in the absorption spectrum may be due to the SPR effect of Ag-NP [30]. Moreover, the

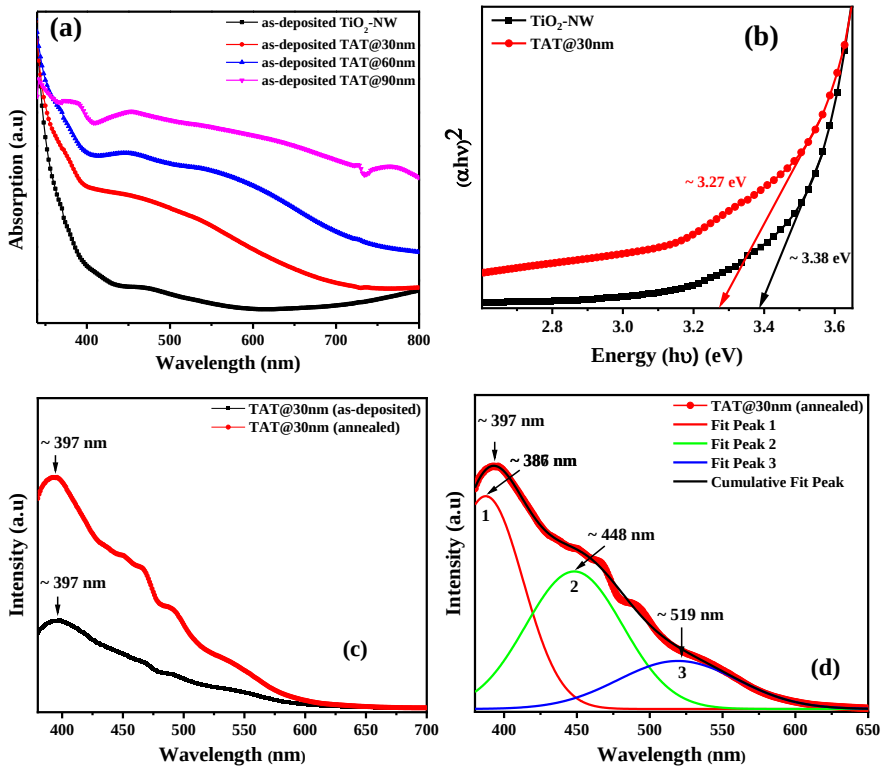

Fig. 5 (a) the optical absorption spectra of as-deposited TiO_2-NW, TAT@30nm, TAT@60nm and TAT@90nm specimens fabricated on the FTO substrate, (b)-the band gap of as-deposited TiO_2-NW and TAT@30nm, (c) PL spectra of as-deposited and annealed TAT@30nm samples and (d) Shows the Gaussian fitted PL graph of annealed TAT@30nm sample

calculated band gaps form the tauc plot of TiO2-NW and TAT@30nm are ~3.38 and ~ 3.27 eV, respectively. Further, room temperature photoluminescence (PL) analysis of the Ag-NP assisted TiO_2-NW sample was done at an excitation wavelength of 340 nm by using a 370 nm stopband filter. The broad PL intensity of the as-deposited and annealed TAT@30nm samples is plotted in Fig. 5 (b). A broad emission peak at ~ 397 nm was observed from as-deposited and annealed TAT@30nm samples.

It was also observed that the PL intensity of the annealed TAT@30nm specimen increased compared to the as-deposited sample, which may be due to the increase in the crystallinity of TiO_2 by reducing the oxygen vacancies. Further, the gaussian fitted curve shows the peaks at ~ 385 nm, ~448 nm, and 519 nm, which correspond to the band-to-band transition of TiO_2 and oxygen defects present between the band gap, as shown in Fig. 5(d).

3.4. Device characterization

The electrical performance of the fabricated DSSCs is characterized at room temperature by using a Source Meter (Keithley 2450) connected to the computer and the photocurrent measurement was taken under light illumination at 100 mW/cm^2 powered by a solar simulator (SS150, Scientech, Canada). Fig. 6 shows the dye absorbed photoanode, counter electrode and DSSC device. The schematic of the DSSC device based on the TAT photoanode is shown in Fig. 6(d). Fig. 7 shows the *J-V* graph of DSSCs based on TiO_2-NW and TAT@30nm photoanodes. And, Table I shows the cell performance of DSSCs devices and the corresponding photovoltaic parameters.

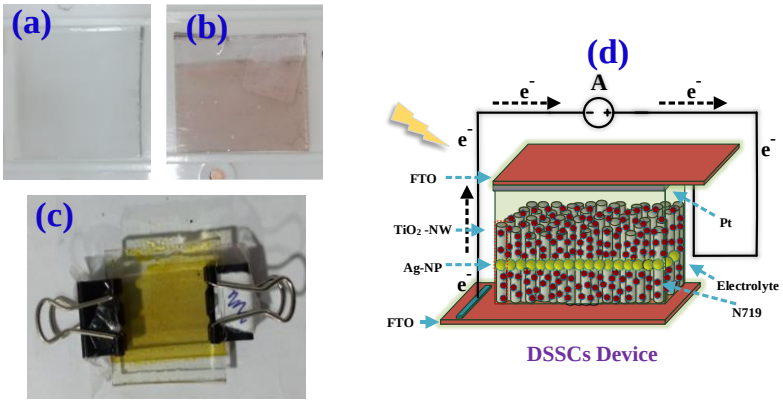

Fig. 6 (a) Fabricated counter electrode, (b) Dye absorbed photoanode and (c) Fabricated DSSC device based on TiO_2-NW photoanode and (d) Schematic of DSSC device based on TAT photoanode

The PCE of the TiO_2-NW is ~ 0.61% and the corresponding open-circuit voltage (V_{oc}) and short circuit current density (J_{sc}) of the cell are ~ 0.51 V and ~ 3.21 mA/cm^2. The efficiency of the DSSCs is reduced to ~ 0.24 percent after the incorporation of Ag nanoparticles, with the corresponding V_{oc} and J_{sc} being ~0.34 V and ~ 2.11 mA/cm^2, respectively. So, there is a difference between the J_{sc} that depends on the light conversion activity and the structure of the photoanode, which determines the electron diffusion PCE

of the solar cell. It is observed that TiO_2-NW photoanode based DSSC devices show better efficiency compared to TAT@30nm photoanode based devices.

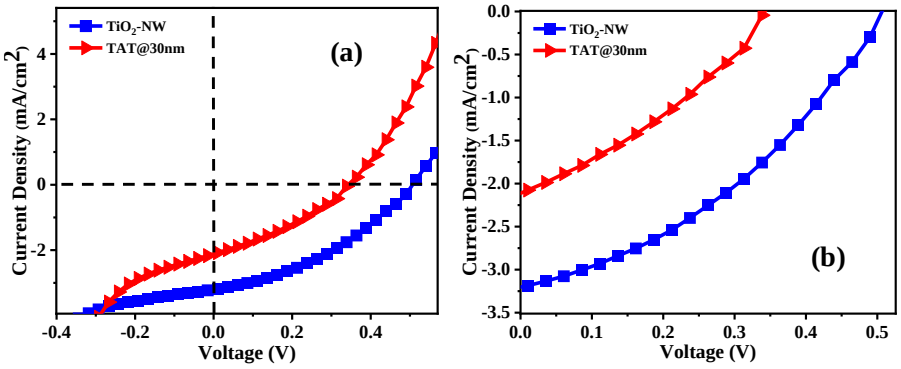

Fig. 7 a) *J-V* graphs of DSSCs based on TiO_2-NW and TAT@30nm photoanode, b) magnified *J-V* graphs of DSSCs

Table 1 Photovoltaic performance of TiO_2-NW and TAT@30nm photoanode based DSSCs

Photoanode	V_{oc} (V)	J_{sc} (mA)/cm^2	V_m (V)	I_m (mA)	*FF*	η %	Reference
MWCNT	0.28	1.76	--	--	0.30	0.15	[31]
ZnO film	0.49	2.15	--	--	0.54	0.56	[32]
TiO_2 film	0.56	1.17	--	--	0.85	0.56	[33]
TiO_2-NW	0.51	3.21	0.32	1.94	0.37	0.61	Our result
TAT@Ag 30 nm	0.34	2.11	0.21	1.13	0.34	0.24	Our result

However, the TiO_2-NW based device improves the accessibility of the entire surface to the dye and corresponding electrolyte medium, leading to a direct and shorter path for the transportation of the electrons. Marquesa *et al.* reported an efficiency of ~ 1.2% from the DSSC fabricated using the tape casting method. It was also observed that the highest efficiency was achieved by using 4-tert-butyl pyridine electrolytes [34]. Again, Erande *et al.* reported a PCE of 0.2% in which the TiO_2 film was deposited using a chemical method [35].The natural dye, acting as a sensitizer of DSSCs, was less efficient. Even so, the efficiency of our DSSC device based on TiO_2-NW was higher than that of DSSCs using natural dye. Furthermore, our device shows better performance in terms of efficiency compared to some of the recently reported devices, as shown in table I. However, the efficiency of our device is still low, which may be due to the small thickness of the photoanode. So, the efficiency may be further improved by increasing the TiO_2-NW photoanode thickness and also by reducing the size of the metal nanoparticles.

4. CONCLUSION

In conclusion, the GLAD method was used to develop TiO_2-NW and Ag-NP-assisted TiO_2-NW photoanodes on an FTO substrate for the development of DSSCs. The SEM and TEM analysis reveal the successful deposition of TiO_2-NW and TAT nanowires. The XRD investigation reveals the presence of Ag-NP and TiO_2 crystals in the samples. The

absorption enhancement from the Ag-NP assisted TiO_2-NW samples observed in the absorption spectrum may be due to the SPR effect of Ag-NP present in the TiO_2-NW. The TiO_2-NW based DSSC device shows better efficiency compared to the Ag-NP assisted TiO_2-NW photoanode based DSSC device. It may be concluded that the size of the Ag-NP incorporation at the mid-point of the TiO_2 NW needs to be reduced to enhance the efficiency of DSSC. Therefore, this presented technique may be employed for developing DSSCs and other optoelectronic device applications.

Acknowledgement: *The authors acknowledge the Department of Science and Technology (DST), Science and Engineering Research Board (SERB), Govt. of India for funding this work under File No. ECR/2018/000834. Also, the authors would like to thank NIT, Durgapur and NIT Nagaland for FE-SEM and XRD analysis, respectively.*

REFERENCES

[1] B. Shougaijam and S. S. Singh, *Growth of Vertically Aligned TiO_2 Nanowire Photoanode for Developing Dye-sensitized Solar Cell*. In: T. R. Lenka, D. Misra, A. Biswas, *Micro and Nanoelectronics Devices, Circuits and Systems. Lecture Notes in Electrical Engineering*, Springer, Singapore, 2023, vol. 904, pp. 119-129.

[2] L. A. Reichertz, I. Gherasoiu, K. M. Yu, V. M. Kao, W. Walukiewicz and J. W. Ager III, "Demonstration of a III-Nitride/Silicon Tandem Solar Cell", *Appl. Phys. Express*, vol. 2, no. 12, p. 122202, Dec. 2009.

[3] W. Chen, Y. Wu, Y. Yue, J. Liu, W. Zhang, X. Yang, H. Chen, E. Bi, I. Ashraful, M. Gratzel and L. Han, "Efficient and stable large-area perovskite solar cells with inorganic charge extraction layers", *Science*, vol. 350, no. 6263, pp. 944-948, Oct. 2015.

[4] S. I. Cha, Y. Kim, K. H. Hwang, Y. J. Shin, S. H. Seo and D. Y. Lee, "Dye-sensitized solar cells on glass paper: TCO-free highly bendable dye-sensitized solar cells inspired by the traditional Korean door structure", *Energy Environ. Sci*, vol. 5, pp. 6071-6075, Jan. 2012.

[5] L. L. Estrella, S. H. Lee and D. H. Kim, "New semi-rigid triphenylamine donor moiety for D-π-A sensitizer: Theoretical and experimental investigations for DSSCs", *Dyes and Pigments*, vol. 165, pp. 1-10, June 2019.

[6] L. L. Estrella and D. H. Kim, "Theoretical design and characterization of NIR porphyrin-based sensitizers for applications in dye-sensitized solar cells", *Sol. Energy*, vol. 188, pp. 1031-1040, Aug 2019.

[7] Q. Miao, M. Wu, W. Guo and Ma. Tingli, "Studies of high-efficient and low-cost dye-sensitized solar cells", *Front. Optoelectron. China*, vol. 4, pp. 103-107, April 2011.

[8] N. Heo, Y. Jun and J. Park, "Dye molecules in electrolytes: new approach for suppression of dye-desorption in dye-sensitized solar cells", *Sci Rep*., vol. 3, pp. 1712, April 2013.

[9] P. Baviskar, A. Ennaoui and B. Sankapal, "Influence of processing parameters on chemically grown ZnO films with low-cost Eosin-Y dye towards efficient dye sensitized solar cell", *Sol. Energy*, vol. 105, pp. 445-454, July 2014.

[10] C. Hora, F. Santos, M. G. F. Sales, D. Ivanou and A. Mendes, "Dye-Sensitized Solar Cells for Efficient Solar and Artificial Light Conversion", *ACS Sustainable Chem. Eng*., vol. 7, pp. 13464-13470, 2019.

[11] S. S. D. Mir, L. E. Liezel, M. A. A. Ivy, L. Anton, M. Nikita, A. Mikaee, N. Massoma, W. Mohebullah, Z. Hameedullah and S. Tomonobu, "Photocatalytic Applications of Metal Oxides for Sustainable Environmental Remediation", *Metals*, vol. 11, pp. 1-25, Jan. 2021.

[12] R. K. Pandey and V. K. Prajapati, "Molecular and immunological toxic effects of nanoparticles", *Int J Biol Macromol*, vol. 107, pp. 1278-1293, Feb. 2017.

[13] R. Allen, "The cytotoxic and genotoxic potential of titanium dioxide (TiO_2) nanoparticles on human SH-SY5Y neuronal cells in vitro", *The Plymouth Student Scientist*, vol. 9, pp. 5-28, 2016.

[14] B. Shougaijam, R. Swain, C. Ngangbam and T. R. Lenka, "Analysis of morphological, structural and electrical properties of annealed TiO_2 nanowires deposited by GLAD technique", *J. Semicond.*, vol. 38, no. 5, p. 053001, May 2017.

[15] R. S. Dubey, K. V. Krishnamurthy and S. Singh, "Experimental studies of TiO_2 nanoparticles synthesized by sol-gel and solvothermal routes for DSSCs application", *Results in Physics*, vol. 14, p. 102390, Sept. 2019.

[16] H. Lee, M. Y. Song, J. S. Jurng and Y. K. Park, "The synthesis and coating process of TiO_2 nanoparticles using CVD process", *Powder Technology*, vol. 214, pp. 64-68. Nov. 2011.
[17] H. K. E. Latha and H. S. Lalithamba, "Synthesis and Characterization of Titanium Dioxide Thin Film for Sensor Applications", *Mater. Res. Express*, vol. 5, p. 035059, March 2018.
[18] H. Y. Yang, M. F Lee, C. H. Huang, Y. S. Lo, Y. J. Chen and M. S. Wong, "Glancing angle deposited titania films for dye-sensitized solar cells", *Thin Solid Films*, vol. 518, pp. 1590-1594, Dec. 2009.
[19] M. S. Wong, M. F. Lee, C. L. Chen and C. H. Huang, "Vapor deposited sculptured nano-porous titania films by glancing angle deposition for efficiency enhancement in dye-sensitized solar cells*", Thin Solid Films,* vol. 519, pp. 1717-1722, Dec. 2010.
[20] J. M. Ji, H. Zhou, Y. K. Eom, C. H. Kim and H. K. Kim, "14.2% Efficiency Dye-Sensitized Solar Cells by Co-sensitizing Novel Thieno [3, 2-b] indole-Based Organic Dyes with a Promising Porphyrin Sensitizer"*, Adv. Energy Mater.,* vol. 10, no. 15, p. 2000124, Feb. 2020.
[21] B. Shougaijam and S. S. Singh, "Structural and optical analysis of Ag nanoparticle-assisted and vertically aligned TiO_2 nanowires for potential DSSCs application", *J Mater Sci: Mater Electron,* vol. 32, pp. 19052-19061, June 2021.
[22] C. Liu, T. Li, Y. Zhang, T. Kong, T. Zhuang, Y. Cui, M. Fang, W. Zhu, Z. Wu and C. Li, "Silver nanoparticle modified TiO_2 nanotubes with enhanced the efficiency of dye-sensitized solar cells", *Micropor. Mesopor. Mat.*, vol. 287, pp. 228-233, Oct. 2019.
[23] B. Pandit, V. S. Devika and B. R. Sankapal, "Electroless-deposited Ag nanoparticles for highly stable energy-efficient electrochemical supercapacitor", *J. Alloys Compd*., vol. 726, pp. 1295-1303, Dec. 2017.
[24] K. V. Alex, P. T. Pavai, R. Rugmini, M. S. Prasad, K. Kamakshi and K. C. Sekhar, "Green Synthesized Ag Nanoparticles for Bio-Sensing and Photocatalytic Applications", *ACS Omega*, vol. 5, no. 22, pp. 13123-13129, May 2020.
[25] N. S. Rohizat, A. H. A. Ripain, C. S. Lim, C. L. Tan, R. Zakaria, "Plasmon-enhanced reduced graphene oxide photodetector with monometallic of Au and Ag nanoparticles at VIS–NIR region", *Sci. Rep*., vol. 11, p. 19688, Oct. 2021.
[26] P. Wen, Y. Han, W. Zhao, "Influence of TiO_2 Nanocrystals Fabricating Dye-Sensitized Solar Cell on the Absorption Spectra of N719 Sensitizer", *Nanotechnol. Solar Energy*, p. 906198, July 2012.
[27] A. Barranco, A. Borras, A. R. González-Elipe and A. Palmero, "Perspectives on oblique angle deposition of thin films: From fundamentals to devices", *Prog. Mater. Sci*., vol. 76, pp. 59-153, March 2016.
[28] S. R. Bhattacharyya, Z. Mallick and R. N. Gayen, "Vertically Aligned Al-Doped ZnO Nanowire Arrays as Efficient Photoanode for Dye-Sensitized Solar Cells", *Journal of Elec Mater.*, vol. 49, pp. 3860-3868, April 2020.
[29] Y. Wang, J. Cheng, M. Shahid, M. Zhang and W. Pan, "A high performance TiO_2 nanowire UV detector assembled by electrospinning", *RSC Adv.*, vol. 7, p. 26220, May 2017.
[30] M. A. K. L. Dissanayake, J. M. K. W. Kumari, G. K. R. Senadeera and C. A. Thotawatthage, "Efficiency enhancement in plasmonic dye-sensitized solar cells with TiO_2 photoanodes incorporating gold and silver nanoparticles", *J. Appl. Electrochem.*, vol. 46, pp. 47-58, Sept. 2016.
[31] P. A. Mithari, A. C. Mendhe, S. S. Karade, B. R. Sankapal and S. R. Patrikar, "MoS_2 nanoflakes anchored MWCNTs: Counter electrode in dye-sensitized solar cell", *Inorganic Chem. Commun.*, vol. 132, p. 108827, July 2021.
[32] A. N. Ossai, S. C. Ezike, P. Timtere and A. D. Ahmed, "Enhanced photovoltaic performance of dye-sensitized solar cells-based Carica papaya leaf and black cherry fruit co-sensitizers", *Chem. Phys. Impact*, vol. 2, p. 100024, April 2021.
[33] N. Purushothamreddy, R. K. Dileep, G. Veerappan, M. Kovendhan and D. P. Joseph, "Prickly pear fruit extract as photosensitizer for dye-sensitized solar cell", *Spectrochimica Acta Part A: Molecular and Biomolecular Spectroscopy*, vol. 228, p. 117686, Oct. 2019.
[34] K. B. Erande, P. Y. Hawaldar, S. R. Suryawanshi, B. M. Babar, A. A. Mohite, H. D. Shelke, S. V. Nipane and U. T. Pawar, "Extraction of natural dye (specifically anthocyanin) from pomegranate fruit source and their subsequent use in DSSC", *Mater. Today: Proc.*, vol. 43, no. 4, pp. 2716-2720, July 2021.
[35] A. S. Marques, V. A. S. Silva, E. S. Ribeiro and L. F. B. Malta, "Dye-Sensitized Solar Cells: Components Screening for Glass substrate, Counter-Electrode, Photoanode and Electrolyte", *Mat. Res.,* vol. 23, no. 5, p. e20200168, Nov. 2020.